TURBO-20-1233

The Effect of Reaction on Compressor Performance

Krishan S. Chana*
Whittle Laboratory
University of Cambridge
Cambridge CB2 1TN, UK
e-mail: kc485@cam.ac.uk

Robert J. Miller
Whittle Laboratory
University of Cambridge
Cambridge CB2 1TN, UK
e-mail: rjm76@cam.ac.uk

Abstract

Reaction is the fundamental parameter by which the asymmetry of the velocity triangle of a stage is set. Little is understood about the effect that reaction has on either the efficiency or the operating range of a compressor. A particular difficulty in understanding the effect of reaction is that the rotor and stator have a natural asymmetry caused by the centrifugal effects in the rotor boundary layer being much larger than that in the stator boundary layer. In this paper a novel approach has been taken: McKenzie's 'linear repeating stage' concept is used to remove the centrifugal effects. The centrifugal effects are then reintroduced as a body force. This allows the velocity triangle effect and centrifugal force effect to be decoupled. The paper shows the surprising result that, depending on how the solidity is set, a 50% reaction stage can either result in the maximum, or the minimum, profile loss. When the centrifugal effects are removed, 50% reaction is shown to minimise endwall loss, maximise stage efficiency and maximise operating range. When the centrifugal effects are reintroduced, the compressor with the maximum design efficiency is found to rise in reaction by 5% (from 50% reaction to 55% reaction) and the compressor with the maximum operating range is found to rise in reaction by 15% (from 50% reaction to 65% reaction).

1 Introduction

In the central stages of a multistage compressor, it is typically argued that symmetrical rotor and stator velocity triangles maximises the stage efficiency. Horlock [1] and Cumpsty [2] say this is because the static-pressure rise is split equally between the rotor and stator and so the adverse pressure gradient is balanced.

There is also an argument for symmetrical velocity triangles maximising stage efficiency based on balancing the relative inlet velocities into the rotor and stator. Denton [3] says that this is because the relative inlet velocities into the rotor and stator are equal. At any other value of reaction, the relative inlet velocities into the rotor and stator are not equal. As the increase in specific entropy due to the surface boundary layers on each blade is proportional to the cube of the surface velocity, the blade with the increased relative inlet velocity will have a greater increase in specific entropy than the reduction in the other blade. There is therefore a reduction in stage efficiency for asymmetric velocity triangles.

These views were the views of the authors until they received a personal communication from Dr L.H. Smith (LHS) on 15th October 2015:

> *'I have found that 50% reaction does not always give the highest efficiency. For a given flow coefficient and work coefficient, 75% reaction gives higher efficiency than 50% reaction. This happens because the lower solidities can be used with high reaction blading, holding* D^*_{eq} *constant.'*

LHS went on to reference a discussion he wrote for Lieblein's paper [4] where he used Lieblein's effective diffusion ratio D^*_{eq} to set the solidity of a stage and this showed that 50% reaction did not produce a compressor with the highest design efficiency. There is further evidence for this by Casey [5] who used a preliminary design system to study the effect of reaction.

In real compressors the reaction is not an independent design variable. This is because at the inlet and exit of a multistage compressor there is zero absolute swirl and this results in high reaction. This corresponds to designs with typically high reactions in the range 70% to 90% [6]. In the central stages of the compressor, it is possible to reduce the reaction to 50% by raising the interstage swirl through the first few stages and dropping it through the last few stages.

However the reaction is chosen, it is important to understand how it effects the overall efficiency and operating range of the compressor. Figure 1 compares the stage velocity triangles for a 50% (symmetric) and 70% reaction design, both with equal flow and work coefficient. It shows why reaction is the fundamental parameter which sets the asymmetry between the rotor and stator velocity triangles.

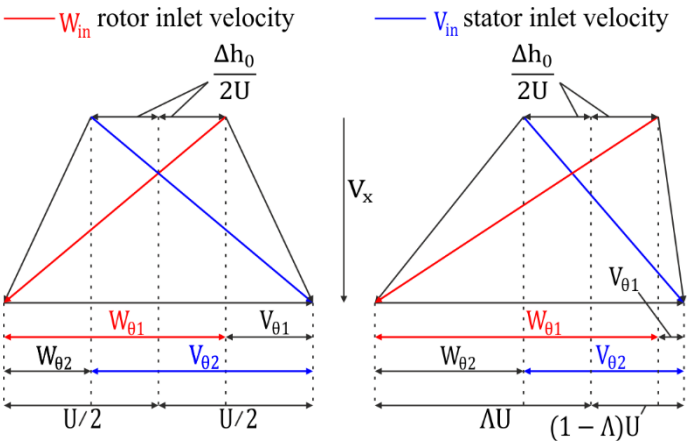

Figure 1: Effect of reaction on velocity triangle asymmetry. LHS: 50% reaction and RHS: 70% reaction.

There is an added natural asymmetry between the rotor and stator caused by rotational forces. This asymmetry is due to two effects of rotation, shown in Figure 2. First, a bulk passage effect, where the centrifugal forces in the freestream are balanced by a radial pressure gradient. This causes the bulk passage flow in the rotor to move radially outward and in the stator to move radially inward. Second, a differential boundary layer effect where the differential effect of centrifugal and Coriolis forces cause the boundary layers in the rotor to be differentially accelerated towards the casing [7]. This effect is critical to this paper as it acts as a natural asymmetry between the way in which the rotor and stator boundary layers develop.

There is some experimental evidence in the literature, [1] [8], to show that high reaction designs are advantageous due to the presence of rotational forces in the rotor. However, in these studies it is difficult to decouple the effects of reaction on the velocity triangle and on the rotational force in the boundary layer, because they are linked. To overcome this problem a new rotation model has been developed which uses the McKenzie's 'linear repeating stage' concept to first remove the effects of rotation. The differential boundary layer effects of rotation are then reintroduced as a body force, in a controlled way.

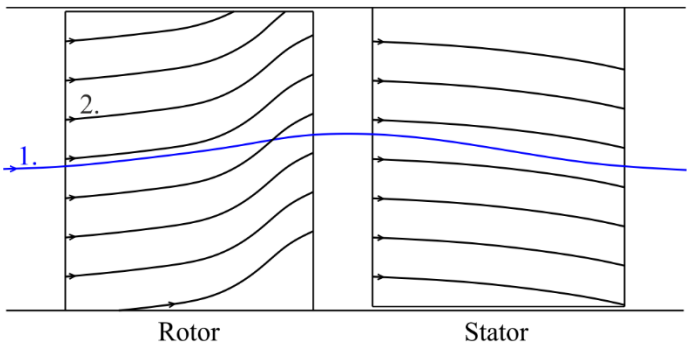

Figure 2: Two effects of rotation: (1) bulk passage effect; and (2) differential boundary layer effect.

In real compressors the choice of reaction also introduces asymmetry into the stage Mach number triangles. For a constant axial velocity ratio, it is thought that 50% reaction maximises the stage efficiency based on balancing the relative inlet Mach numbers into the rotor and stator. This becomes more important as the Mach numbers increase due to the increased peak Mach numbers on the rotor and stator and increased shock losses. To decouple the effects of reaction from the effects of Mach number in this study, a blade speed Mach number of 0.3 was chosen so that the flow can be considered incompressible.

This paper is split into three parts. First the effect of reaction on profile loss is investigated. Second the effect of reaction on the endwall with rotation switched off is investigated. Finally, the effect of reaction on the endwall with rotation switched on is investigated.

2 Methodology

The performance of a compressor stage is a function of many non-dimensional parameters. In this paper, the number of parameters is reduced for simplicity so that the effect of reaction and rotation can be studied in isolation. The design is limited to the typical design choices available to a compressor designer trying to design the central stages of a multistage compressor. Equation 1 describes the typical choices available:

$$(\psi', \eta) = f(\Phi_d, \Psi_d, \Lambda_d, M_u, \sigma, AR, t/c, \varepsilon/c, Re_c) \qquad (1)$$

In this paper a design flow coefficient Φ_d of 0.597 and work coefficient Ψ_d of 0.436 is chosen, these values are the same as used by To & Miller [9]. The blade speed Mach number M_u is set to 0.3. The aspect ratio AR is set as 2.0. The values of t/c and ε/c are fixed as 0.05 and 0.01 respectively. The stage length is constant, which fixes the rotor and stator Reynolds numbers Re_c. At 50% reaction the rotor and stator Re_c are equal to 10^6. The remaining design choices are described by equation 2:

$$(\psi', \eta) = f(\Lambda_d, \sigma) \qquad (2)$$

where Λ_d is the design reaction and σ is the solidity of the stage. It will be shown that the optimal choice of reaction depends on the way in which the solidity is set. In this paper three different methodologies of setting solidity will be used: (1) by fixing the solidity, (2) by fixing the equivalent diffusion ratio D_{eq}^* equal to 1.78 [4] or (3) by fixing the shape factor of the suction-surface boundary layer at the blade trailing edge H_{te}. These three methodologies have common values at 50% reaction, where the level of solidity is set to achieve a diffusion factor of approximately 0.45. Appendices A and B explain how the solidity is set using fixed D_{eq}^* and H_{te}.

2.1 CFD Setup. The 2-D loss calculations in this paper are computed using the program MISES, a coupled Euler boundary layer solver [10]. The boundary layers are considered to be fully turbulent.

The 3-D loss calculations are computed using the program TBlock, a multi-block structured grid Computation Fluid Dynamics (CFD) program developed by John Denton [11]. TBlock is a fully 3-D, Reynolds-Averaged Navier-Stokes (RANS) finite volume program. Steady mixing planes are used and the boundary layers are considered to be fully turbulent.

The aerofoil geometries are of a controlled diffusion aerofoil type, designed using MISES so that the stagnation streamline always bifurcates on the nose of the aerofoil. The aerofoils are designed with a 'linear shape factor philosophy' where the suction-surface shape factor increases from the peak suction point to the trailing edge linearly. The compressor designs are cantilevered with a plane annulus. The rotor tip and stator hub clearances are equal and set to 1% of the aerofoil chord length hence 50% reaction rotor and stator geometries are identical.

2.2 Linear Repeating Stage Model. Smith [12] showed that in a multistage compressor the spanwise stage inlet conditions repeat after three to four stages in a well-matched compressor. McKenzie [6] developed this into a 'linear repeating stage' concept and it has been implemented computationally by Auchoybur & Miller [13] and To & Miller [9]. There are two elements to its implementation in this paper.

First the bulk passage effect of rotation is removed by choosing a compressor geometry which is at a span-to-radius ratio of 0, i.e. the rotor and stator are rectilinear cascades of blades. This allows coupled-influence between the rotor and stator and removes the variation in velocity triangles up the span.

Secondly a 1.5 stage compressor model (rotor-stator-rotor) is calculated using 3-D CFD. The stator exit conditions are copied to the rotor inlet and this is repeated at the beginning of each timestep. This means that in each converged calculation the stator exit conditions are identical to the rotor inlet conditions.

2.3 Rotation Model. A central part of this paper is the ability to switch on and off rotational forces in a controlled way. The effects of rotation are first removed by choosing a compressor geometry which is at a span-to-radius ratio of 0.

As described above the rotational forces have two effects. First, the bulk passage effect and second a differential boundary layer effect. This second effect is critical to this study as it acts as an asymmetry between the way in which the rotor and stator boundary layers develop.

It was decided that the rotation model should only model the differential boundary layer effect. This is because the bulk passage effect causes small incidence variations across the span of the blade. In a real design the blade profile would be varied along its span to compensate for this effect. In this controlled study, detailed redesign of the blade across the span must be avoided and so it was decided that the bulk passage effects of rotation would not be modelled.

To model only the differential boundary layer effect, the rotation model adds a body force per unit volume into the CFD calculation of the form:

$$\left.\frac{\rho V_\theta^2}{r} - \frac{\overline{\rho V_\theta^2}}{r}\right|_{(x,r)} \tag{3}$$

This new term models the perturbation centrifugal forces. The second term in equation 3 is defined as the pitchwise volume-averaged value of $\rho V_\theta^2/r$ at the same meridional position i.e. the same axial and radial coordinates and r is an effective radius. The new model was introduced into TBlock as a source term:

$$\rho\frac{DV_r}{Dt} - \rho\left(\frac{V_\theta^2}{r} - \left.\frac{\overline{V_\theta^2}}{r}\right|_{(x,r)}\right) = -\frac{\partial p}{\partial r} + \text{viscous} + F_r \tag{4}$$

The model allows an effective radius to be set. By setting a high value, the blades act as if part of a rectilinear cascade. By setting the effective radius equal to the radius of a real compressor the perturbation centrifugal forces are equal to those in a real compressor. The benefit of using the model, rather than changing the real radius of the compressor, is that the geometry of the stage remains unchanged as the magnitude of the body force is varied.

3 Profile Loss

The lost efficiency of a stage due to profile loss alone can be written as:

$$\frac{T\Delta s}{\Delta h_0} = \frac{(T\Delta s)_{rotor} + (T\Delta s)_{stator}}{\Delta h_0} \tag{5}$$

where T, for an incompressible case, is the temperature at stage exit and Δh_0 is the rise in stagnation enthalpy across the stage.

The total entropy generation in the attached boundary layer on each blade, either rotor or stator, can be calculated by integrating the entropy production in the boundary layer over the blade surface:

$$\dot{S} = \sum c\left[\int_0^1 C_d \rho \frac{V_0^3}{T}\frac{dx}{c}\right] \tag{6}$$

where the summation is across both blade surfaces and V_0 is the velocity at the boundary layer edge. Writing equation 6 in the form of the lost efficiency of a row of blades gives:

$$\left(\frac{T\Delta s}{\Delta h_0}\right)_{row} = 2\frac{C_0}{V_x}\sum \sigma \underbrace{\left(\frac{V_{in,ref}}{C_0}\right)^3}_{\text{2. Velocity triangle term}} \underbrace{\left[\int_0^1 C_d\left(\frac{V_{0,ref}}{V_{in,ref}}\right)^3\frac{dx}{c}\right]}_{\text{3. Single blade loss coefficient}} \tag{7}$$

1. Solidity

where we follow Denton [3] and write the enthalpy change in terms of an isentropic stage reference velocity C_0:

$$C_0 = 2\sqrt{\Delta h_0} \quad (8)$$

and $V_{in,ref}$ is the relative inlet velocity into the blade row.

The lost efficiency given by equation 7, is made up of three terms. The first term, the solidity, represents the effect of changing the number of blades in a row. The second term represents the effect of changing the velocity triangle on loss. This term is high for a blade row with a high relative inlet velocity. It shows that one of the key aims for a designer is to minimise the ratio of the cube of the relative inlet velocity into the blade rows relative to the enthalpy rise of the stage. The third term is the single blade loss coefficient. This term is high if a blade has a high surface velocity, relative to the blade inlet velocity, or a large wetted area.

In the following section, the three terms in equation 7 will be used as a framework through which we can understand the effect of reaction on the lost efficiency of a stage. It will be shown that changing reaction changes all three terms. Only by controlling how these terms change with reaction can the effect of reaction on the lost efficiency of a stage be understood.

3.1 Constant Solidity. It is commonly believed that compressors of 50% reaction have the highest stage efficiency. This way of thinking is based on the idea that the blade solidity is held constant. The lost efficiency of each blade row for the case of constant solidity is plotted in Figure 3. The shape of each line is mainly determined by changes in term 2 in equation 7, the velocity triangle term. Moving from 50% to 70% reaction, term 2 changes by approximately +60% and term 3 changes by -7%. The shape of the lines is caused by the way in which the velocity triangle controls the relative inlet velocity into each blade row and the fact that loss scales with the cube of the relative inlet velocity into the blade row. The black line in Figure 4 shows the lost efficiency of this stage. It is clear that 50% reaction must be the most efficient stage because it minimizes the sum of the $V_{in,ref}^3$ into both blade rows. The variation in lost efficiency is

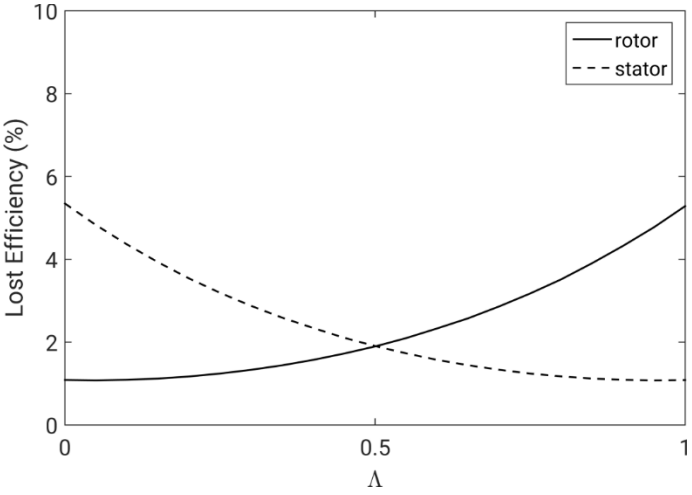

Figure 3: Blade row lost efficiency for the case of constant solidity and blade loss coefficient (MISES).

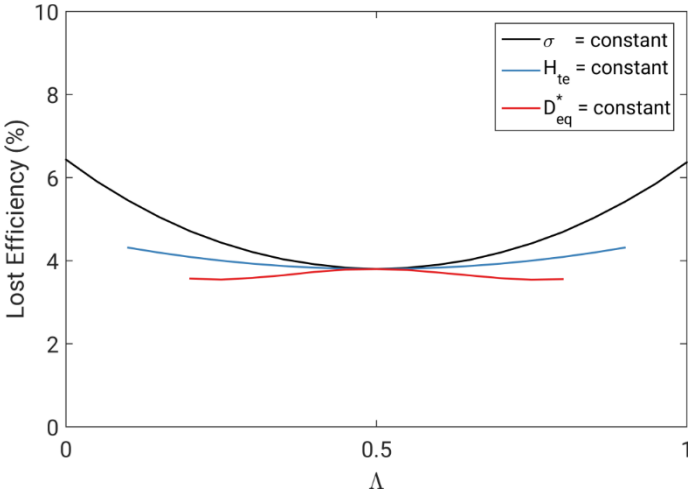

Figure 4: Stage lost efficiency for the cases of constant solidity, D_{eq}^* and H_{te} (MISES).

symmetrical about 50% reaction. Increasing reaction from 50% to 70% reduces the stage efficiency by 0.39%.

3.2 Effect of Solidity. The view developed in the previous section was the view of the authors until they received the personal communication from LHS quoted previously. In this section the solidity is controlled in two ways. First, as LHS proposed, the equivalent diffusion ratio D_{eq}^* of each blade row is held constant. Second, the shape factor of the suction-surface boundary layer at the trailing edge H_{te} of each blade row is held constant.

The effect of holding the equivalent diffusion ratio D_{eq}^* constant and equal to 1.78 is shown as the red line in Figure 4. The change in the solidity is shown in Figure 5. The line shows that, as LHS said, 50% reaction is now the most inefficient compressor. In fact, at 50% reaction the compressor has an efficiency which is 0.22% lower than an equivalent compressor at 70% reaction. Figure 5 shows that this is caused by dropping the solidity in both the rotor and stator by approximately 60%. It seems surprising that the solidity in both blade rows drops simultaneously. This effect will be explained later in the section.

The effect of holding the shape factor of the suction-surface boundary layer at the trailing edge H_{te} constant is shown as the blue line in Figure 4. The line shows that the change in lost efficiency is almost independent of reaction. Increasing reaction from 50% to 70% reduces the stage efficiency by only 0.13%. Figure 5 shows that increasing reaction from 50% to 70% reduces the solidity in both blade rows by approximately 30%.

It is clear that as LHS said, solidity plays an important role in determining the impact of reaction on compressor efficiency. However, to understand this effect, a choice must be made about how the solidity is varied as the design of the blade is changed.

To understand why there is a reduction in rotor and stator solidity either side of 50% reaction, we will consider the diffusion factor DF equation [14] in its simplest form:

$$DF = 1 - DH + \frac{\Delta V_\theta}{2V_{in}\sigma} \quad (9)$$

where DH is the blade row de Haller number. In this analysis the diffusion factor DF will be considered instead of the equivalent diffusion factor D^*_{eq} as it is of similar form but is simpler, giving a clearer physical explanation of the underlying mechanisms. Rearranging equations 9 gives:

$$\sigma = \frac{\Delta V_\theta / 2V_{in}}{DF - (1 - DH)} \quad (10)$$

We can then define the top and bottom of equation 10 as two terms given by equations 11 and 12:

$$\text{term } 1 = \Delta V_\theta / 2V_{in} \quad (11)$$

and

$$\text{term } 2 = DF - (1 - DH) \quad (12)$$

Term 1 represents a loading term relative to the relative inlet velocity into the blade row. Term 2, for a fixed diffusion factor DF equal to 0.45, is proportional to the blade row de Haller number DH. Figures 6 and 7 show the variation of term 1 and term 2, defined by equations 11 and 12, relative to their values at 50% reaction for the rotor and stator respectively. The maximum solidity occurs when the two lines meet at a tangent. This occurs at approximately 50% reaction.

Term 1, in Figure 6, varies almost linearly with reaction. The reason for this is that the work coefficient and blade speed are constant so that ΔV_θ is constant. However, as the reaction rises, the relative inlet velocity into the rotor V_{in} rises. This steady rise in V_{in} causes the approximately linear rise in term 1.

Term 2, in Figure 6, varies almost parabolically with reaction. This variation is driven by the variation in de Haller

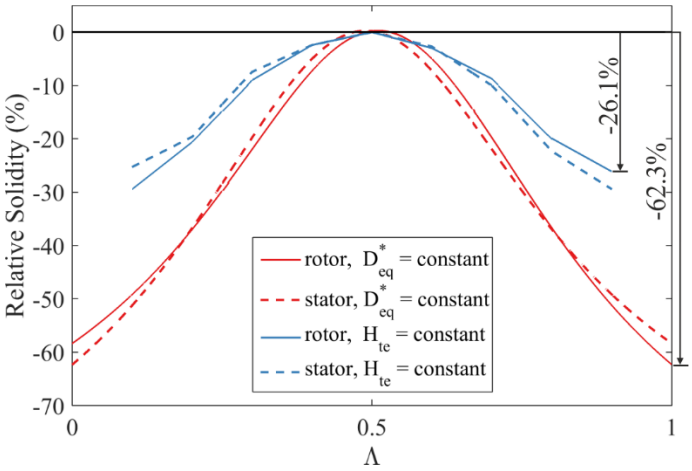

Figure 5: Reduction in solidity relative to 50% reaction for the cases of constant D^*_{eq} and H_{te} (MISES).

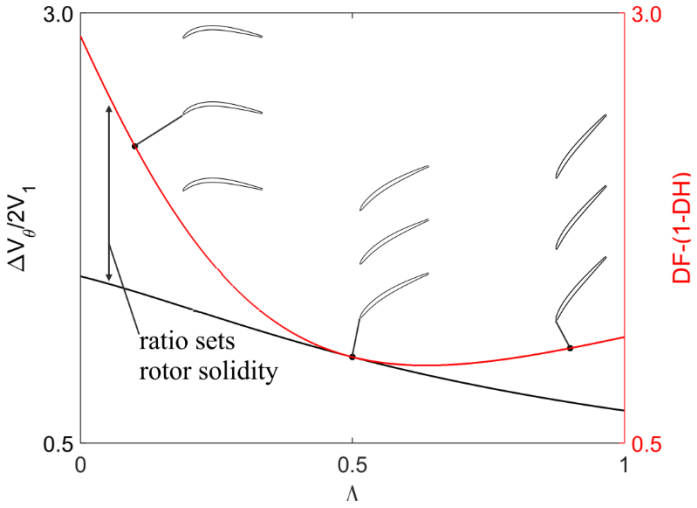

Figure 6: Change in term 1 and term 2 relative to 50% reaction for the rotor.

number DH. One might expect that as reaction is increased, the rotor DH would continually drop, but it does not. Above a reaction of approximately 60% it starts to rise again. This is because as reaction rises, the rotor static-pressure rise continually increases, however V_{in} also increases. The two effects combine to set DH. As reaction increases beyond approximately 60%, the increase in static-pressure rise across the rotor is weak relative to the increase in V_{in}. This results in the de Haller number rising. The inflection point in term 2 is at a reaction of approximately 60%, however, the gradient of term 1 results in the two lines meeting at a tangent at approximately 50% reaction. Looking once again at Figure 5 we can see that for the case of constant D^*_{eq} and constant H_{te} the maximum solidity occurs close to, but not quite at, 50% reaction.

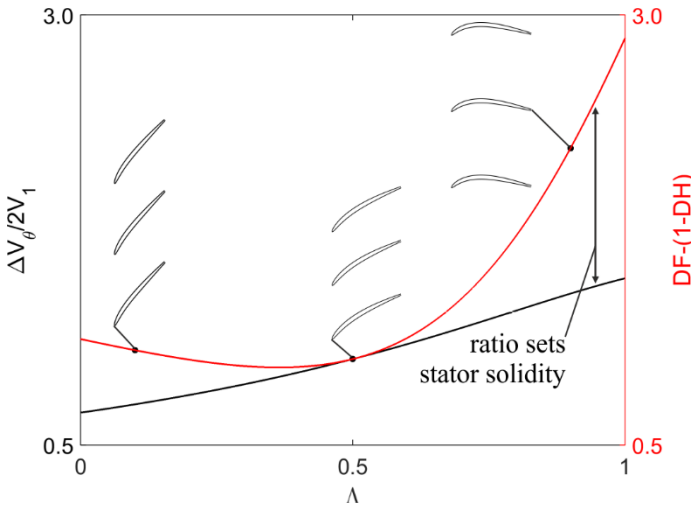

Figure 7: Change in term 1 and term 2 relative to 50% reaction for the stator.

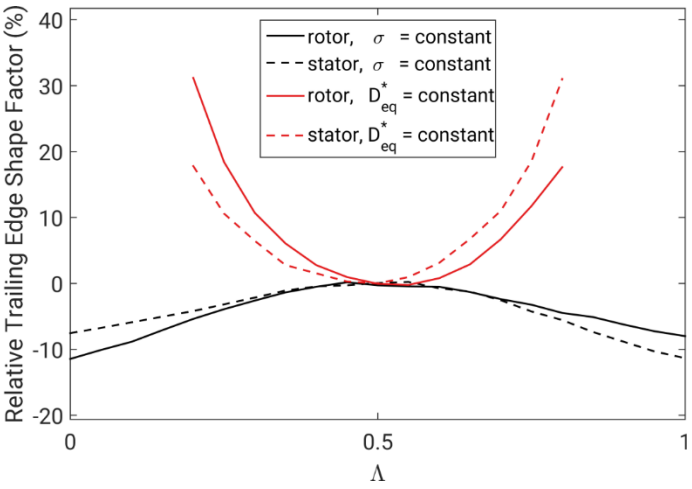

Figure 8: Change in suction-surface trailing edge shape factor relative to 50% reaction for the cases of constant solidity and D^*_{eq} (MISES).

Finally, Figure 8 shows how the shape factor of the suction-surface boundary layer at the trailing edge H_{te} changes with reaction, for the case of constant solidity and constant equivalent diffusion ratio D^*_{eq}. It is clear that setting D^*_{eq} constant is undesirable because as the reaction moves away from 50% the boundary layers are driven toward separation. Equally it is clear that holding solidity constant is undesirable because as the reaction moves away from 50% the stage becomes over bladed.

3.3 Effect of Work and Flow Coefficient. It is clear from the previous section that whether 50% reaction is the most, or least, efficient compressor depends on a trade between the solidity effect (term 1 in equation 7) and the velocity triangle and blade loss coefficient effects (term 2 and term 3 in equation 7). This trade depends on the particular work and flow coefficient at which the compressor is designed. Whether 50% reaction is the most, or least, efficient compressor therefore depends on where on the Smith Chart a stage is located. The aim of this paper is not to explore the effect of changing work and flow coefficient, however, the effects for the cases of constant solidity and constant D^*_{eq} are easily calculated and will be discussed to highlight the sensitivity of changing work and flow coefficient.

Figure 9 shows the case of constant solidity and Figure 10 shows the case of constant D^*_{eq}. The contours show the difference in the efficiency between a compressor of 70% reaction and a compressor of 50% reaction. Blue means that 50% reaction is most efficient and red means that 50% reaction is the least efficient. The variation of lost efficiency with reaction at the three points A, B and C in both Figures 9 and 10 are shown in Figure 11. Appendix C explains how the lost efficiency is calculated for these cases. The black dotted lines are lines of constant de Haller number at 50% reaction.

From Figures 9 and 10 a number of points can be made. First, as the work and flow coefficient are raised, point C, in both Smith Charts, is a blue region. This implies that in this region the 50% reaction compressor is more efficient than the 70% reaction compressor by approximately 0.31% for the case of constant solidities and 1.08% in the case of constant D^*_{eq}.

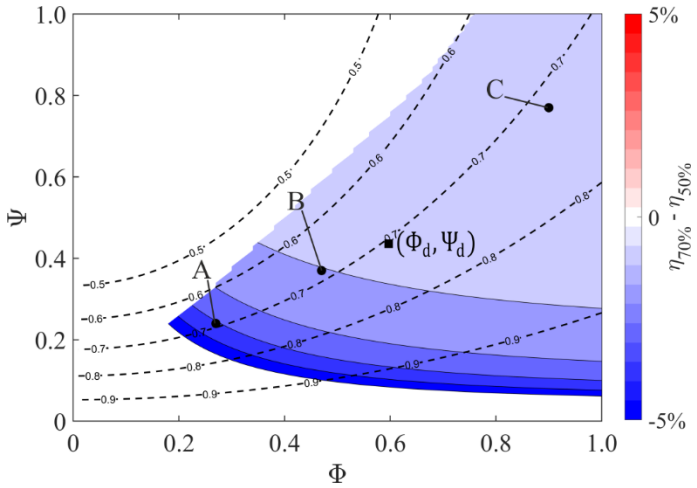

Figure 9: Smith Chart showing the effect of reaction on efficiency for the case of constant solidity.

Second, the region close to the work and flow coefficient explored earlier in this paper, point B, the effect of reaction is very sensitive to how the designer selects solidity. By changing the way the solidity is set, 50% reaction can switch between the most, and the least, efficient compressor.

Finally, as the work and flow coefficient are dropped, point A, both Smith Charts once again show a blue region. This shows that the 50% reaction compressor is more efficient than the 70% reaction compressor. In fact, for the case of constant solidity, a 50% reaction compressor is shown to be approximately 3.11% more efficient than a 70% reaction compressor.

The results indicate that it would be worth future studies investigating the effect of varying the reaction at other work and

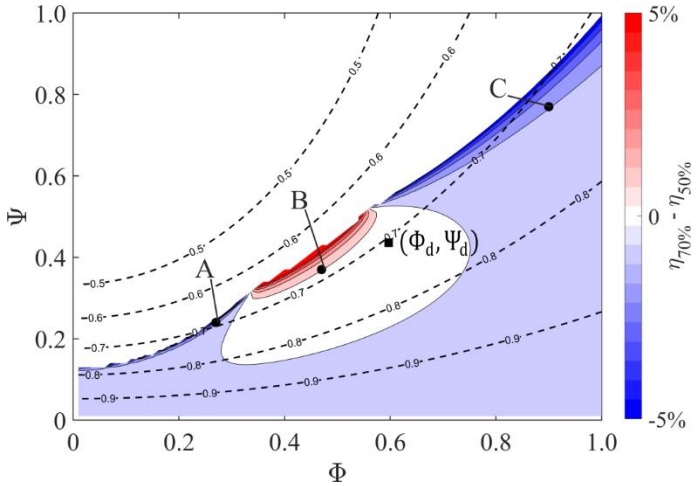

Figure 10: Smith Chart showing the effect of reaction on efficiency for the case of constant D^*_{eq}.

flow coefficients on the Smith Chart. These studies should consider both profile and endwall loss to assess the maximum efficiency in an accurate way.

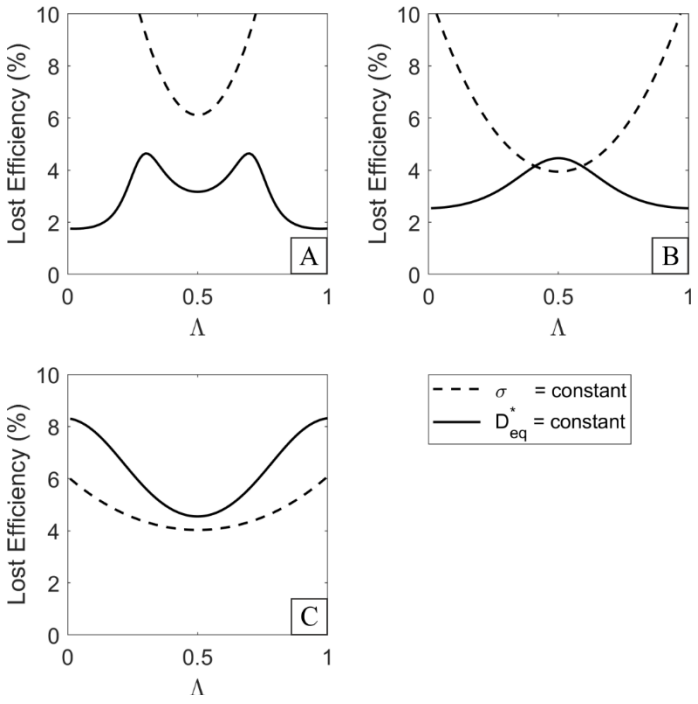

Figure 11: Variation of stage lost efficiency with reaction at points A, B and C in Figures 9 and 10.

4 Endwall loss with Rotation Model Switched Off

In this section the effects of reaction on the endwall loss, with the rotational model switched off, are presented. The solidity of both the rotor and the stator have been set by fixing the boundary layer shape factor at the trailing edge of the suction-surface H_{te}. The compressor is cantilevered with the hub endwall rotating, connected to the rotor, and the casing endwall stationary connected to the stator. The endwall loss is defined as the total loss minus the profile loss.

4.1 Design Loss. The effect of reaction on the hub endwall loss is shown in Figure 12. The black line shows the case with zero clearance and the red line shows the case with a 1% stator hub clearance. For clarity, the casing endwall loss has not been plotted. It is identical to the hub endwall loss except that the x axis is one minus reaction, $1 - \Lambda$. The hub endwall loss can be seen to rise as reaction rises.

The cause of the rise can be understood by considering the loss which would occur in a turbulent boundary layer over the hub endwall. The boundary layer edge velocity is considered to vary axially, and to be equal to the circumferentially mass-averaged blade mid-span rotor relative velocity $W(x)$. The rotor relative velocity is chosen because the hub endwall rotates with the rotor. The entropy generation rate in the rotating hub endwall boundary layer, per unit pitch, is therefore given by equation 13:

$$\dot{S} = \int \frac{C_d \rho W^3(x)}{T} dx \qquad (13)$$

where the value of C_d is set as 0.002 [3]. Writing equation 13 in the form of the hub lost efficiency gives the blue line in Figure 12. The exact form of the equation plotted is derived in Appendix D. A comparison of the blue and black line shows that the rise in loss, as the reaction is raised, is caused by the rise in the rotor relative velocity.

The cause of the rise in the rotor relative velocity, as the reaction is raised, can be understood from the velocity triangles in Figure 1. As the reaction is raised, the relative velocity into both the rotor and the stator, W_1 and W_2, can be seen to rise. Another way to understand the effect of reaction on the rotor relative velocity is by considering the time-averaged rotor relative streamline at mid-height, shown in Figure 13. To a first order, the relative flow angle is set by the stagger of the rotor. As the reaction is raised, the stagger of the rotor is raised and therefore the relative flow angle rises. As the mid-height axial velocity is held constant, as the reaction rises, the rotor relative velocity also rises.

A secondary effect of reaction on endwall loss can be seen in Figure 12. Comparing the black line, the case where the stator has no clearance gap between it and the rotating hub endwall, and the red line, the case where the stator has a 1% clearance gap, it can be seen that the stator hub leakage loss drops as the reaction is raised. This is because as the reaction is raised the stator stagger is reduced, shown as the dashed line in Figure 13.

Figure 14 shows the effect of reaction on the total lost efficiency of the stage. For both the cases without and with rotor and stator clearances, the 50% reaction compressor is the most efficient. Table 1 summarises the results in Figure 14 by comparing the difference in lost efficiency between the 70% and 50% reaction stage. As expected from the findings earlier in this paper, fixing solidity by setting a constant H_{te}, results in the profile loss of the stage becoming relatively independent of reaction. Table 1 shows that changing reaction from 70% to 50% reduces the endwall lost efficiency, causing an increase in stage

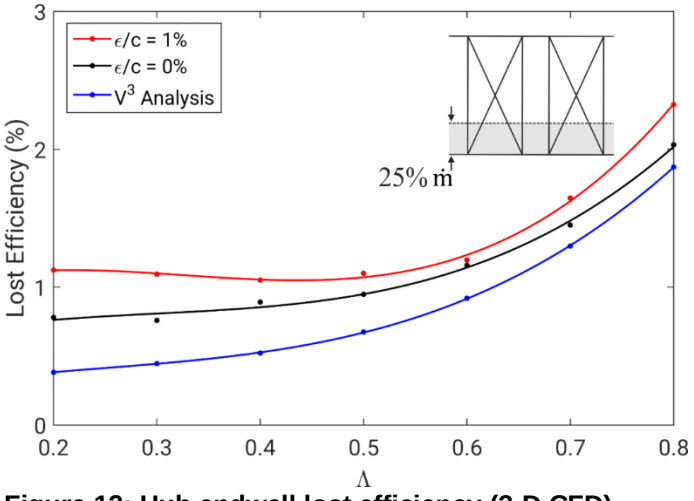

Figure 12: Hub endwall lost efficiency (3-D CFD).

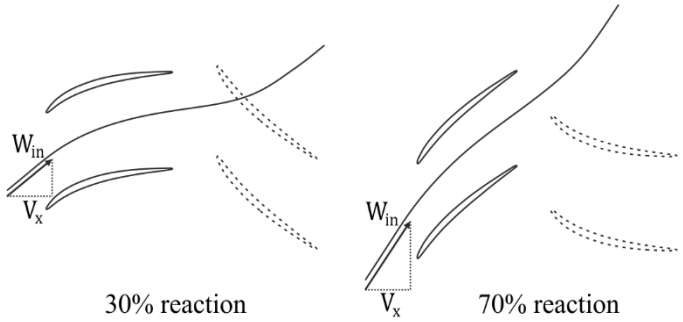

Figure 13: Mid-span streamline in the rotor relative frame for 30% (left) and 70% (right) reaction.

efficiency of 0.49%, for the case with clearances, and 0.58%, for the case without clearances.

Table 1: Summary of the effect of reaction on design efficiency (constant H_{te}, 3-D CFD).

$\eta_{\Lambda=70\%} - \eta_{\Lambda=50\%}$ (%)	0% clearances	1% clearances
Endwall	-0.47	-0.38
Profile	-0.11	-0.11
Total	-0.58	-0.49

4.2 Operating Range. The effect of reaction on the operating range of the compressor, for the cases without clearances and with clearances, are shown in Figures 15 and 16. On each plot, the dotted line shows the maximum pressure rise throttle characteristic at the point at which the CFD solution started to diverge.

To compare the operating range between compressors, the maximum pressure rise throttle coefficient, k, is used. This is a measure of the exit area at maximum pressure rise and is defined in equation 14.

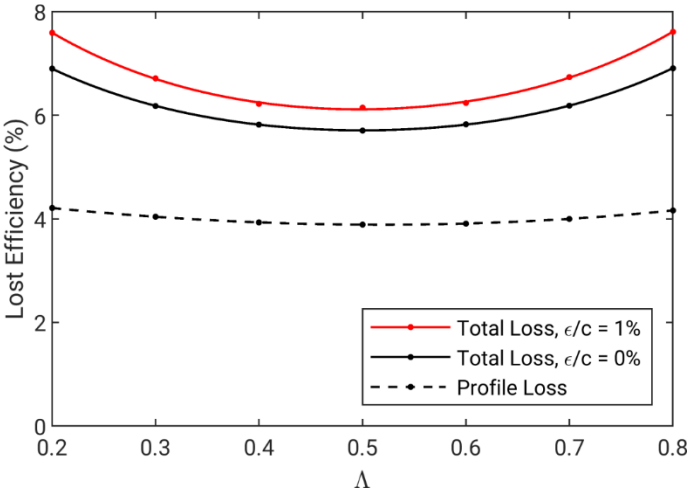

Figure 14: Variation of lost efficiency with reaction for the case of solidity set by constant H_{te} (3-D CFD).

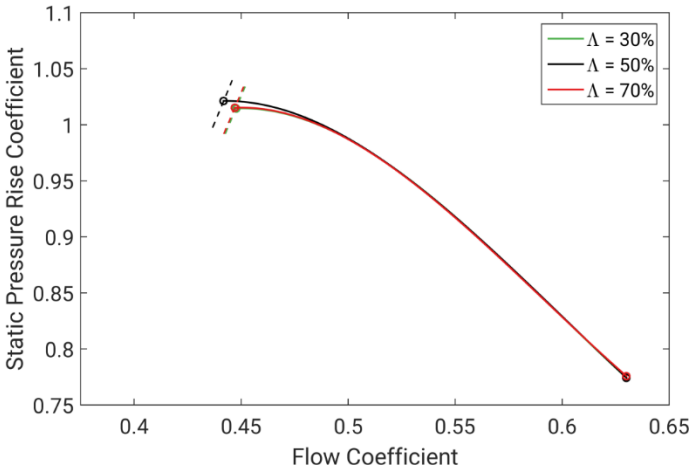

Figure 15: Static-pressure rise characteristics for compressors without clearances (constant H_{te}, 3-D CFD).

$$k = \frac{\psi'}{\Phi^2} \tag{14}$$

Figure 17 gives a summary of how the maximum pressure rise throttle coefficient k varies with reaction. For both cases, the 50% reaction compressor has the largest operating range. It can be seen that the addition of clearances reduces the operating range at all reactions, by a similar amount.

The cause of the reduction in the maximum pressure rise throttle coefficient, as the reaction is raised, can be seen in Figure 18. The figure shows the limiting surface streamlines at close to maximum pressure rise for the stator of the 50% and 70% reaction compressor stages, without clearances. As the reaction is raised the size of the stator hub corner separation can be seen to increase. It is this increase which causes the reduction in the maximum static-pressure rise throttle coefficient. It may seem unexpected that the size of the stator hub corner separation rises

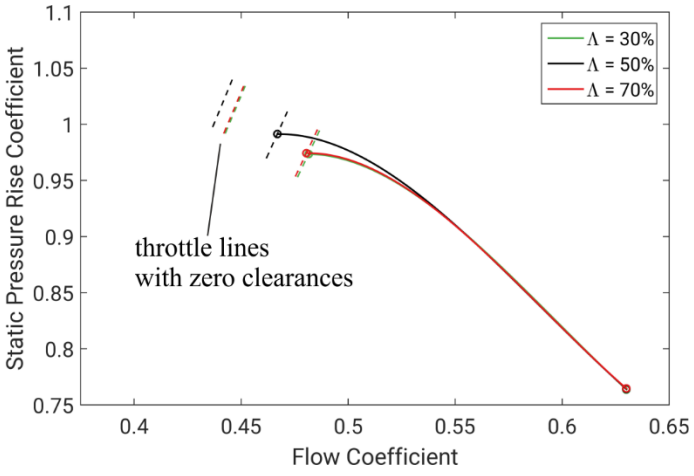

Figure 16: Static-pressure rise characteristics for compressors with clearances (constant H_{te}, 3-D CFD).

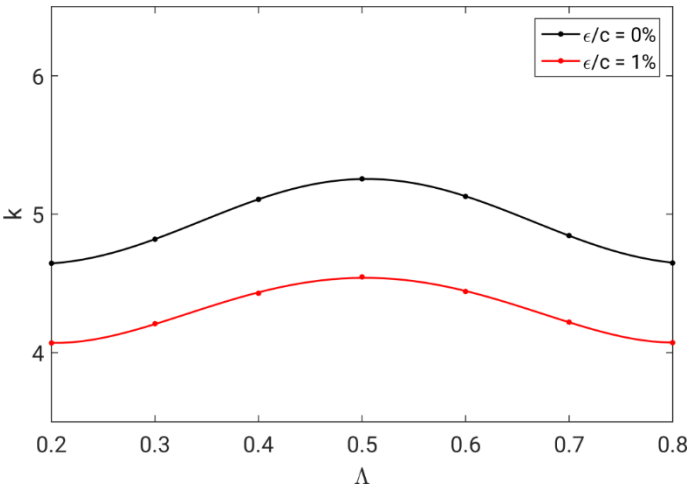

Figure 17: Maximum pressure rise throttle coefficient (constant H_{te}, 3-D CFD).

as the reaction is increased, as the pressure rise across the stator drops. This will be explained later in the section.

The cause of the reduction in the maximum pressure rise throttle coefficient, as the reaction is reduced below 50%, shown in Figure 17, is similar to the cause of the reduction in the maximum static-pressure rise throttle coefficient at high reaction, discussed above. As the reaction is reduced below 50% the size of a rotor casing corner separation increases, reducing the maximum static-pressure rise throttle coefficient. This case is not shown for brevity.

The cause of the increase in the size of the stator hub corner separation at high reaction can be understood by looking at the spanwise distribution of the local static-pressure rise coefficient across the stator, shown in Figure 19. Here we follow Auchoybur and Miller [13] and define the local static-pressure rise coefficient C_p as:

$$C_p = \frac{\Delta p}{\frac{1}{2}\rho V_{local}^2} \qquad (15)$$

where V_{local} is the relative inlet velocity to the stator. The

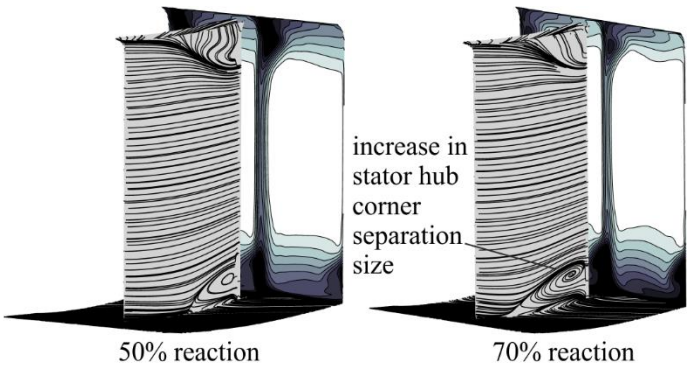

Figure 18: Stator suction-surface limiting streamlines for the case of zero clearances (constant H_{te}, 3-D CFD).

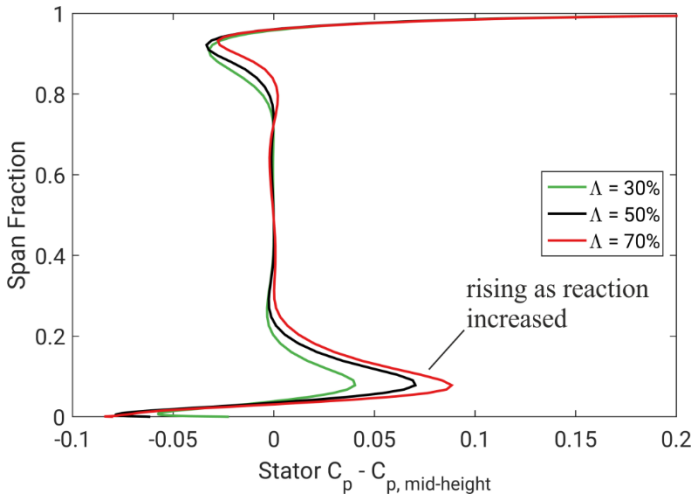

Figure 19: Spanwise variation in stator static-pressure rise with zero clearance (constant H_{te}, 3-D CFD).

denominator of equation 15 is the inlet dynamic pressure into the stator at each span fraction. Figure 19 shows that as the reaction is raised the C_p in the stator hub rises. This is the cause of the rise in the size of the stator hub separation.

It should be noted that in the case considered, the variation in blade speed up the blade span has been deliberately removed. The increase in C_p close to the stator hub region is caused by the repeating stage endwall boundary layer that has developed in the multistage environment. In a real compressor, where the blade speed varies up the span, there would be an additional inviscid effect caused by the reaction variation up the blade span.

The increase in C_p in the stator hub region, as the reaction is raised, is caused by a drop in stator inlet velocity, V_{local} in equation 15. The cause of this drop can be understood by looking at the stator inlet velocity triangle. This shows the re-energising effect, caused by the change in frame of reference, described by Koch [15] and Auchoybur and Miller [13].

Figure 20 shows the freestream and hub endwall stator inlet velocity triangles for 30% and 70% reaction. The freestream and hub endwall velocities have been extracted from the CFD by mass-averaging the velocities over 25% to 75% of the mass flux and 0% to 25% of the mass flux respectively. The figure shows that as the reaction rises from 30% to 70% the relative difference between V_{fs}^2 and V_{hub}^2 rises, causing an increase in the relative difference between the freestream C_p and the hub endwall C_p.

The cause of this drop in V_{hub}^2 relative to V_{fs}^2, as the reaction is raised can be understood from Figure 20. As the reaction is increased the axial velocity in the endwall region drops. In addition, at higher reactions, the magnitude of V_{fs}^2 is lower and therefore any drop in V_{hub}^2 causes a larger fractional change in the difference between V_{hub}^2 and V_{fs}^2.

Finally, it is necessary to explain why the axial velocity in the hub endwall region drops as the reaction is raised. Consider once again the hub streamtube (0% to 25% of the mass flux) used

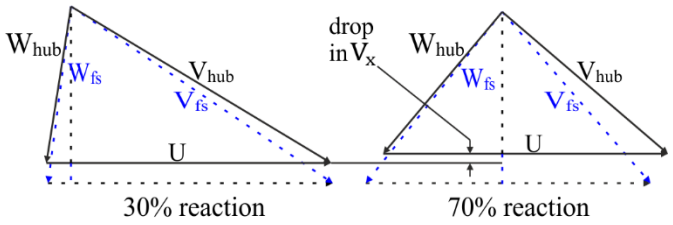

Figure 20: Stator inlet velocity tringles for hub endwall (solid) and freestream (dashed) regions.

to create Figure 20. Now the mass-averaged change in stagnation enthalpy, stagnation pressure and the entropy across the stage is extracted from the CFD. As the flow is incompressible the three are related by the fundamental thermodynamic relation:

$$\frac{\Delta h_0}{U^2} = \frac{\Delta p_0}{\rho U^2} + \frac{T_0 \Delta s}{U^2} \qquad (16)$$

In the endwall region there are two restrictions on equation 16. First, the second term, the stagnation pressure rise coefficient, must be constant as reaction is changed, shown in the left-hand side of Figure 21. This is because in a repeating stage the stagnation-pressure rise coefficient is constant across the span and all the stages have been designed to achieve the same stagnation-pressure rise coefficient.

Second, the first term in equation 16, the work coefficient, must always collapse onto the same characteristic, shown in the right-hand side of Figure 21. This is because as the reaction of a compressor is changed the gradient of its work coefficient verses flow coefficient characteristic does not change. This is true in the freestream but it was also found to be true in the endwall region. This is because the deviation in the endwall region is small, approximately 1°, and is relatively independent of reaction. In practice this means that in the endwall regions, as the reaction is changed, the stage moves along a fixed characteristic.

The consequence of the restrictions on the stagnation-pressure rise coefficient and the work coefficient, discussed above, can be seen in Figure 21. As the reaction rises, the hub endwall loss rises. This causes the design point of the compressor to move to a higher work coefficient and a lower flow coefficient. The consequence of this reduction in flow coefficient in the endwall region is a drop in the axial velocity, shown for the 70% reaction compressor in Figure 20. This results in the rise in the static-pressure rise coefficient shown in the hub region in Figure 19.

It should be noted that the connection between an increase in endwall loss and a reduction in endwall flow was also observed by Auchoybur and Miller [13]. Auchoybur and Miller showed that a rise in loss in the hub endwall region resulted in a lowered flow in that region, and a consequential reduction in the maximum pressure rise throttle coefficient of the compressor. However, they went on to show that by redesigning the velocity triangle in the endwall region the flow in that region could be increased, raising the maximum pressure rise throttle coefficient of the compressor. Their work therefore implies that by

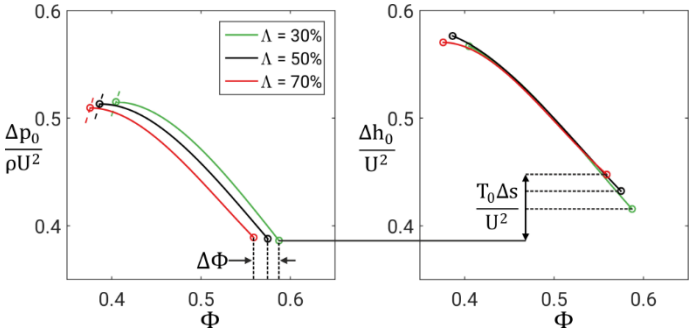

Figure 21: Stagnation-pressure rise (left) and work coefficient (right) characteristics for hub endwall region.

redesigning the velocity triangle in the endwall region of high reaction compressors, the reduction in the maximum pressure rise throttle coefficient, shown in Figure 17, could be recovered.

To summarise, the reduction in the maximum pressure rise throttle coefficient of a stage, as the reaction is raised, is caused by an increase in the hub endwall loss and is shown in Figure 17. The rise in loss results in a reduction of flow in the endwall region and a subsequent increase in the static-pressure rise coefficient across the hub of the stator, shown in Figure 19. This causes the size of the stator hub corner separation to increase, shown in Figure 18, and the maximum pressure rise throttle coefficient of the stage to drop.

The behaviour described is fundamental to all cantilever compressors. However, it should be noted that in this study the blade speed has been deliberately held constant across the span. In a real compressor it will vary causing the reaction to vary between the blade root and tip. This does not change the physical process described in this section, but means that when the mid-height reaction is set, the designer must be aware that the casing and hub endwalls will operate at slightly different reactions.

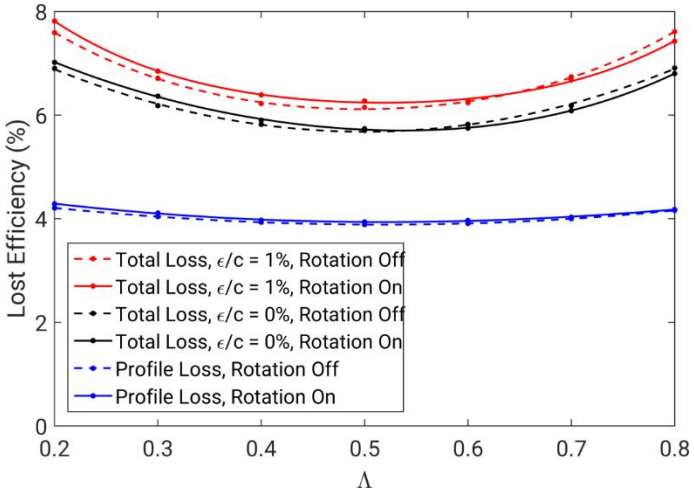

Figure 22: Change in lost efficiency for cases with rotation switched on and off (constant H_{te}, 3-D CFD).

5 Endwall loss with Rotation Model Switched On

This section will investigate the effect of centrifugal forces on the efficiency and operating range of a compressor. The centrifugal forces equivalent to a real compressor of hub-to-tip ratio equal to 0.8 have been introduced by switching on the rotation model.

5.1 Design Loss. The effect of rotation on the total lost efficiency of the stage is shown in Figure 22. It can be seen that rotation has a relatively small effect on design loss. However, the reaction which achieves the optimal design efficiency increases by around 5% reaction (from 50% reaction to 55% reaction). It is also important to note that the range of reactions over which the efficiency only varies by 0.01% is relatively wide, between 50% reaction and 60% reaction.

5.2 Operating Range. The effects of rotation on the operating range of a compressor are much larger than the effect on design loss. Figures 23 and 24 show the effect of switching on the rotation model on compressors with and without clearances. The effect of switching the model on, on the maximum pressure rise throttle coefficient is shown in figures 25 and 26. The effect is to increase the reaction which achieves the maximum pressure rise, by around 15 points (from 50% reaction to 65% reaction).

The effect of switching on rotation on the surface limiting streamlines is shown in Figures 27 and 28. The figures show the compressor at a flow coefficient which is just before maximum pressure rise ($\Phi = 0.449$). The figures show that the effects of rotation are much larger in the rotor than in the stator.

It is useful to understand how the size of the centrifugal forces on the boundary layer change through the rotor and stator. To do this a dimensionless parameter is defined, the dimensionless perturbation centrifugal force F_c, which is a measure of the relative magnitude of the perturbation centrifugal forces in the boundary layer.

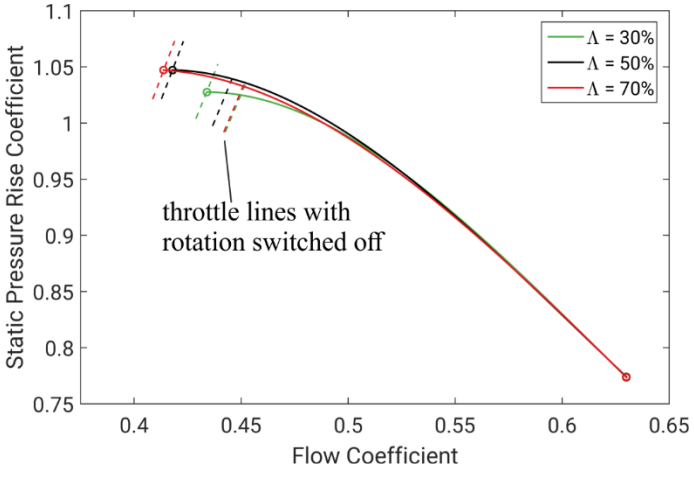

Figure 23: Static-pressure rise characteristics for compressors without clearances and rotation on (constant H_{te}, 3-D CFD).

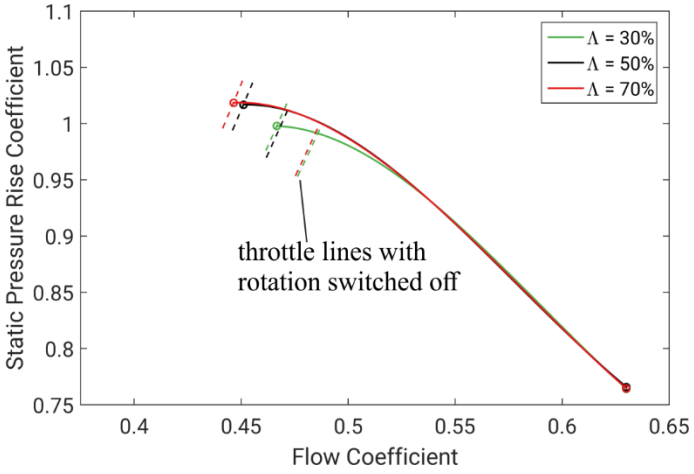

Figure 24: Static-pressure rise characteristics for compressors with clearances and rotation on (constant H_{te}, 3-D CFD).

The dimensionless perturbation centrifugal force F_c is defined as the difference between the centrifugal force, per unit volume, of the fluid on the surface of the blade ($\rho U^2/r$ for the rotor and 0 for the stator) and that in the local freestream $\rho V_\theta^2/r$, non-dimensionalised by the blade speed squared U^2, density ρ and the blade span Δr. This gives the dimensionless perturbation centrifugal force F_c as:

$$F_c = \frac{\rho\left(\frac{V_\theta^2}{r}\right)_{surface} - \rho\left(\frac{V_\theta^2}{r}\right)_{fs}}{\rho U^2/\Delta r} = \frac{\Delta r}{r}\left(\frac{\Delta V_\theta^2}{U^2}\right) \qquad (17)$$

The first term on the right-hand side of equation 17, $\Delta r/r$, controls the overall magnitude of the perturbation centrifugal forces in the stage. This shows that if a stage has a low span-to-radius ratio, $\Delta r/r \to 0$, then the perturbation centrifugal forces in the boundary layer approach zero. This term can also be rewritten as the hub to tip ratio of the compressor.

The second term on the right-hand side of equation 17, $\Delta V_\theta^2/U^2$, varies across the blade surfaces and is a measure of the relative local magnitude of the perturbation centrifugal forces in the boundary layer. For the rotor this second term can be written as:

$$\frac{\Delta V_\theta^2}{U^2} = \frac{U^2 - (V_\theta^2)_{fs}}{U^2} \qquad (18)$$

because the fluid on the rotor blade surface moves at the blade velocity. For the stator, it can be written as:

$$\frac{\Delta V_\theta^2}{U^2} = \frac{0 - (V_\theta^2)_{fs}}{U^2} \qquad (19)$$

because the fluid on the stator blade surface is stationary. The terms on the right-hand side of equation 18 and 19 and the left-

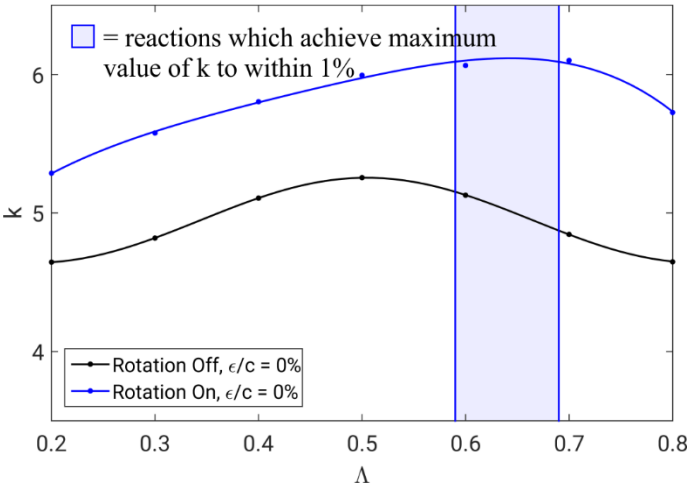

Figure 25: Throttle coefficients for cases with zero clearances and rotation switched on and off (constant H_{te}, 3-D CFD).

hand side of equation 18 and 19 are shown in Figure 29. This shows that the boundary layers on the rotor centrifuge radially outwards, and the boundary layers on the stator centrifuge radially inwards.

Figure 30 shows the effect of changing reaction on the centrifugal effects in the boundary layers. As the reaction is raised above 50%, the strength of the centrifuging of the rotor boundary layers outwards rises, and the strength of the centrifuging of the stator boundary layers inwards drops.

We can now explain why switching on the rotational model causes the maximum pressure rise throttle coefficient at high reaction to increase. In the previous section it was shown that at high reaction the maximum pressure rise throttle coefficient was controlled by a corner separation in the stator hub. Figure 31

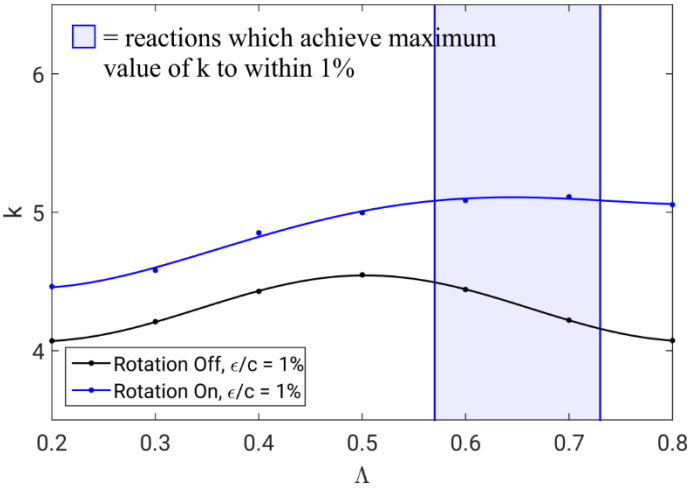

Figure 26: Throttle coefficients for cases with 1% clearances and rotation switched on and off (constant H_{te}, 3-D CFD).

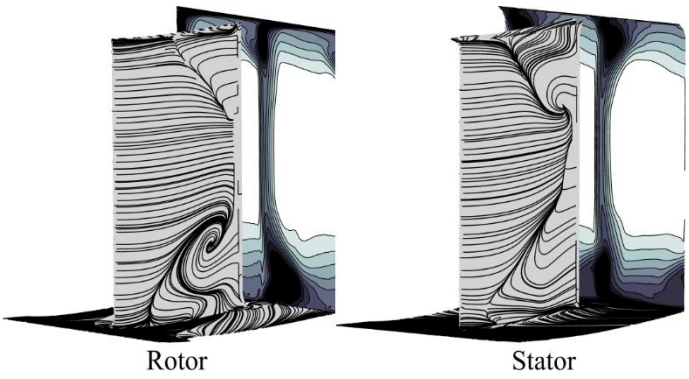

Figure 27: Suction-surface limiting streamlines for 50% reaction with rotation switched off (constant H_{te}, 3-D CFD).

shows that at 70% reaction, switching on the rotational model causes a large reduction in the size of this corner separation. The reason for this can be seen in Figure 32. At 70% reaction, switching on the rotational model, causes the static-pressure rise coefficient across the stator hub to drop. The reason for this is that switching on the rotational model causes the boundary layers in the rotor to centrifuge radially outward, transporting high loss fluid away from the hub endwall. This in turn increases the flow through the hub endwall region reducing the static-pressure rise coefficient across the stator hub.

5.3 Effect of Varying Level of Rotation. The effect of varying the level of rotation on the maximum pressure rise of the compressor is shown in Figure 33. The figure shows the effect of changing the effective radius of the compressor from 0.03% of a real compressor (a rectilinear cascade) to 250% of a real compressor. The figure shows that the increase in the maximum pressure rise occurs when the effective radius changes between approximately 25% and 125% of a real compressor.

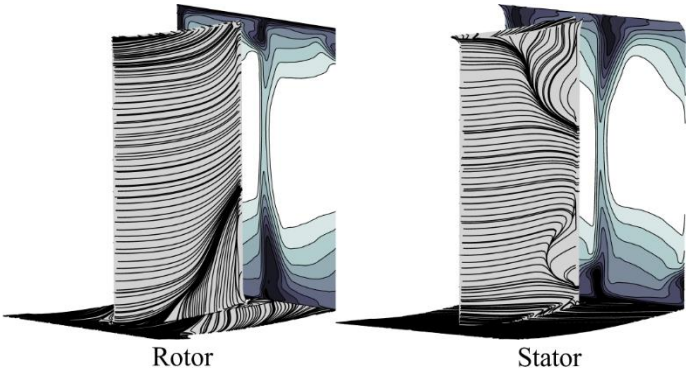

Figure 28: Suction-surface limiting streamlines for 50% reaction with rotation switched on (constant H_{te}, 3-D CFD).

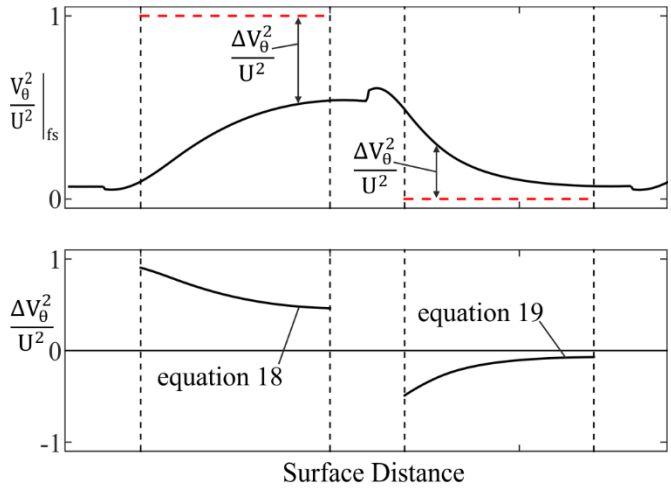

Figure 29: Differential boundary layer effect of rotation for 50% reaction (constant H_{te}, 3-D CFD).

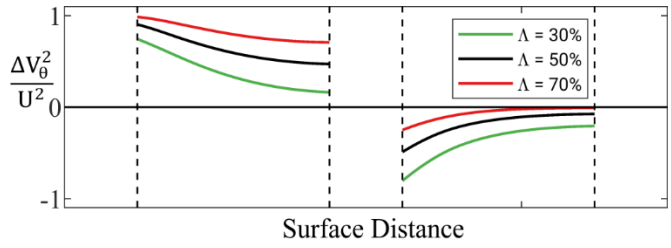

Figure 30: Differential boundary layer effect of rotation (constant H_{te}, 3-D CFD).

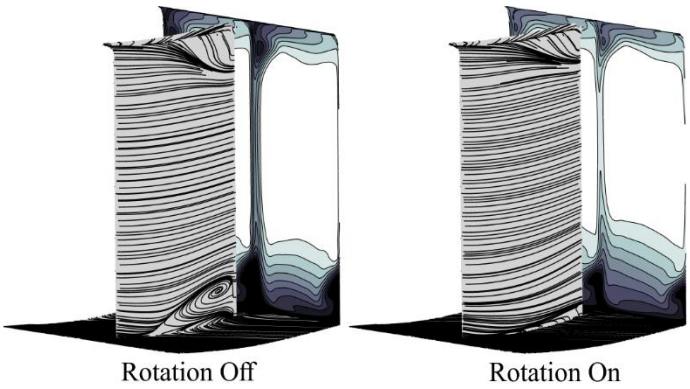

Figure 31: Stator suction-surface limiting streamlines for 70% reaction without clearances (constant H_{te}, 3-D CFD).

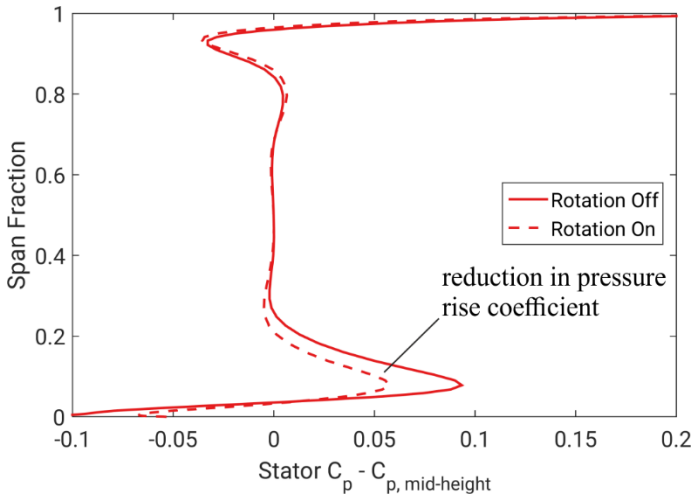

Figure 32: Spanwise variation of stator static-pressure rise for case of 70% reaction (constant H_{te}, 3-D CFD).

6 Application to Multistage Compressors

We are now in a position to understand how the choice of reaction affects the overall lost efficiency of a multistage core compressor. This is an important industry question because the requirement for axial flow at the inlet and exit of a multistage compressor naturally results in high reaction. The designer therefore must decide whether to tolerate this high reaction through the compressor or to aim for a more optimal reaction in the central stages of the compressor.

To answer this question the lost efficiency of a multistage machine can be written as:

$$\left(\frac{T\Delta s}{\Delta h_0}\right)_{compressor} = \frac{\sum_1^n (T\Delta s)_{stage}}{\Delta h_0} \qquad (20)$$

where the summation of loss is across all n stages and Δh_0 is the isentropic work input to the machine. We will consider a hypothetical $n = 10$ stage compressor, with axial flow at the inlet and exit. For conventional levels of work (Ψ_d=0.436) and flow coefficient (Φ_d=0.597), axial flow at the inlet and exit of the compressor corresponds to a reaction of approximately 75%. The lost efficiencies found in this paper can be used in equation 20 to estimate the overall lost efficiency of a multistage compressor.

To understand how the choice of reaction affects the overall lost efficiency we will consider three cases. The stagewise distribution of reaction in these three cases is shown in Figure 34.

Case A represents a historic design philosophy of having 50% reaction in all the stages. To achieve this, the inlet swirl to the first stage must be set by an upstream Inlet Guide Vane (IGV) and the outlet swirl must be removed using an Outlet Guide Vane (OGV) is required. This adds additional loss. We will consider the loss coefficient of the IGV and OGV to be 0.04, a typical value for this type of configuration.

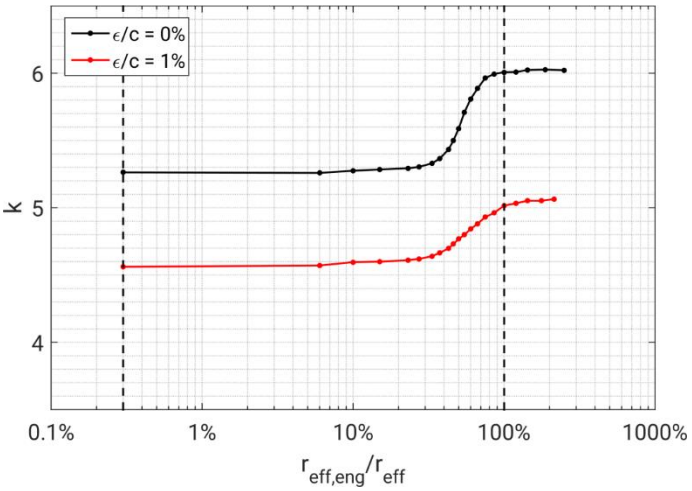

Figure 33: Throttle coefficients for cases with varying level of rotation (constant H_{te}, 3-D CFD).

Case B represents a second historic design philosophy where the reaction is maintained at 75% through all stages. This benefits from having no IGV or OGV, however, it suffers from having a reaction which has a higher design loss. Using the design lost efficiency from Figure 22, this case has a design efficiency which is 0.07% higher than case A. It should be noted that this design philosophy would have a better operability than Case A, due to the increased maximum pressure rise of its stages. This explains why many historic compressors, with high reactions, had a relatively good design efficiency and operating range.

Case C represents the compressor with the maximum design efficiency. This has central stages which have a reaction of 55%, which was shown in section 5.1. This case has a design efficiency which is 0.65% higher than case A.

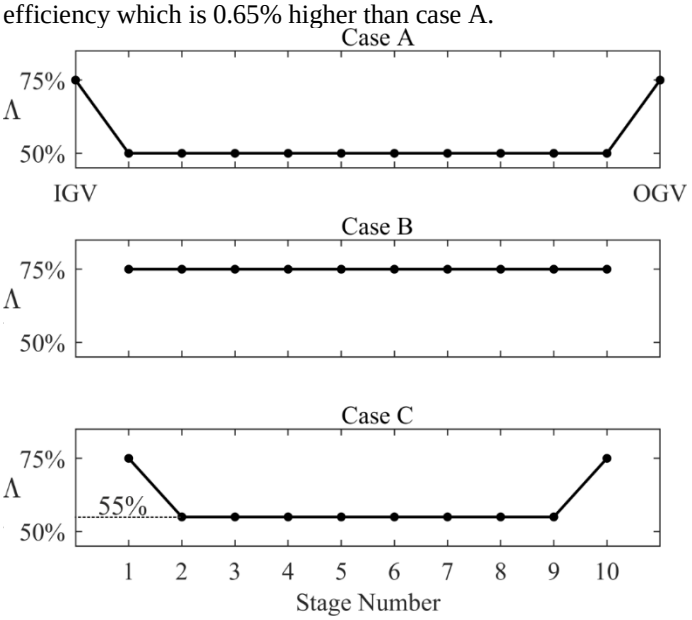

Figure 34: Comparison of four stagewise distributions of reaction for a 10 stage compressor.

Of the three cases, case C resulted in the highest design efficiency, however, it is important to note that if the central stages have an efficiency between 50% and 60% the change in efficiency is relatively small. This provides the designer with a useful degree of freedom.

7 Conclusions

There is considerable debate over the effect of reaction on compressor design efficiency and operating range. This study shows that the confusion is due in part to the inability to decouple the effects of the centrifugal force and the effects of changing the velocity triangle, in a controllable way.

The effect of reaction on profile loss has been shown to be highly dependent on the methodology by which the solidity is set. When the solidity is set by the shape factor of the suction-surface boundary layer at the blade trailing edge, and conventional levels of work and flow coefficient are used (Ψ=0.436 and Φ=0.597), the profile loss has been shown to be independent of reaction.

Reaction is shown to have a major effect on endwall loss. This is because it controls the freestream velocity of the flow relative to the endwall, at the edge of the endwall boundary layer. When the centrifugal effects are removed 50% reaction compressors have the lowest endwall loss and thus the highest design efficiency.

The maximum pressure rise capability of high reaction compressors is limited not by the rotor, but by the stator. This is counterintuitive because at high reaction the pressure rise in the rotor is greater than in the stator. The cause of this is due to the way reaction changes endwall loss, and the way reaction changes the re-energising effect provided by the change in reference frame, descibed by Koch [15] and Auchoybur and Miller [13].

When the centrifugal forces are reintroduced, the compressor with the maximum design efficiency is found to rise in reaction by 5 points (from 50% reaction to 55% reaction) and the compressor with the maximum operating range is found to rise in reaction by 15 points (from 50% reaction to 65% reaction). If a designer aims to maximise the design efficiency of a compressor, the reaction of its central stages should therefore be 55%. However, it is important to note that the maximum efficiency is a weak function of reaction between reactions of 50% and 60%.

Currently, many preliminary design systems do not differentiate between rotors and stators in terms of loss and operating range. This means that they are unlikely to correctly predict the true optimal reaction. In addition, the high centrifugal forces in the rotor boundary layers, relative to those in the stator, implies that the three-dimensional design of rotors should differ from that of stators and should incorporate centrifugal effects.

The study shows that Dr L.H. Smith's statement that reactions higher than 50% were optimal was correct. However, it has been shown that his reasoning was incorrect and that the primary cause is the asymmetry in the magnitude of the perturbation centrifugal forces in the rotor and stator boundary layers.

It is interesting to note that historically high reaction compressors operated with relatively high design efficiency and operating range. This paper gives an explanation of why this could be the case.

It is also interesting to note that high reaction stages have lower optimal blade solidities. This significantly reduces the number of blades in the compressor. This implies that in the future, high reaction compressors could be optimal in applications where cost and weight are the primary drivers.

Acknowledgement

The authors would like to thank John Denton, Chris Hall, Nick Cumpsty, Simon Gallimore, Tom Hynes, Tony Dickens, James Taylor, Ho-On To, John Adamczyk and Dr L.H. Smith (LHS) for their support throughout this project. The authors would also like to thank Rolls-Royce plc. and the Engineering and Physical Sciences Research Council (EPSRC) for funding this work.

Nomenclature

Symbols

c	=	chord
k	=	throttle coefficient
p	=	pressure
r	=	effective radius
t	=	blade maximum thickness
T	=	temperature
U	=	rotor blade speed
V	=	absolute velocity
W	=	relative velocity
Δh_0	=	change in specific stagnation enthalpy
Δr	=	blade span
Δs	=	change in specific entropy
AR	=	aspect ratio
C_d	=	dissipation coefficient
C_0	=	isentropic stage reference velocity
C_p	=	local static-pressure rise coefficient
D^*_{eq}	=	equivalent diffusion ratio
DF	=	diffusion factor
DH	=	de Haller number
F_c	=	perturbation centrifugal force
F_r	=	radial force
H_{te}	=	trailing edge boundary layer shape factor
M_u	=	Mach number based on blade speed
Re_c	=	Reynolds number based on chord
$\dot{S}$	=	entropy creation

Subscripts

0	=	stagnation
1	=	rotor inlet
2	=	stator inlet
bl	=	boundary layer
d	=	design
fs	=	freestream
in	=	inlet
x	=	axial
θ	=	circumferential

Greek Symbols

Φ	=	flow coefficient
Ψ	=	work coefficient
Λ	=	reaction
ε	=	clearance
ψ'	=	static-pressure rise coefficient
η	=	isentropic efficiency
σ	=	solidity

References

[1] J. H. Horlock, Axial flow compressors, London: Butterworths & Co, 1958.

[2] N. A. Cumpsty, Compressor aerodynamics, London: Longman Scientific & Technical, 1989.

[3] J. D. Denton, "Loss mechanisms in turbomachines," *J. Turbomach,* vol. 115(4), Oct 1993.

[4] S. Lieblein, "Loss and stall analysis of compressor cascades," *J. Basic. Eng,* vol. 81(3), Sep 1959.

[5] M. V. Casey, "A mean line prediction method for estimating the performance characteristic of an axial compressor stage," in *IMechE Paper C264/87*, 1987.

[6] A. B. McKenzie, Axial flow fans and compressors, London: Ashgate, 1997.

[7] J. H. Horlock and J. Wordsworth, "The three-dimensional laminar boundary layer on a rotating helical blade," *J.Fluid. Mech,* vol. 23(2), Oct 1965.

[8] C. D. Farmakalides, A. B. McKenzie and R. L. Elder, "The effect of reaction on axial flow compressor performance," in *Proc. ASME. GT1994, Volume 1: Turbomachinery*, The Hague, Netherlands, Jun 1994.

[9] H. To and R. J. Miller, "The effect of aspect ratio on compressor performance," *J. Turbomach,* vol. 141(8), Aug 2019.

[10] M. Drela and H. Youngren, "A user's guide to MISES version 2.6," 2008.

[11] J. D. Denton, "TBlock description and user manual version 15.1," 2015.

[12] L. H. Smith, Casing boundary layers in multistage axial flow compressors, Flow research on blading, Amsterdam: Elsevier, 1970.

[13] K. Auchoybur and R. J. Miller, "Design of compressor endwall velocity triangles," *J. Turbomach,* vol. 139(6), Jun 2017.

[14] S. Lieblein, "Diffusion factor for estimating losses and limiting blade loadings in axial-flow-compressor blade elements," NACA research memorandum, Cleveland, Ohio, Jun 1953.

[15] C. C. Koch, "Stalling pressure rise capability of axial flow compressor stages," *J. Eng. Power,* vol. 103(4), Oct 1981.

[16] H. To, "The effect of aspect ratio on compressor performance," University of Cambridge, U.K, PhD thesis, 2016.

Appendix A: Setting Solidity using D_{eq}^{*}

Holding constant the equivalent diffusion ratio $D_{eq}{}^{*}$ [4] in equation A1 allows the blade row solidity σ to be set. This requires knowledge of the stage velocity triangles only.

$$D_{eq}{}^{*} = \frac{1}{DH}\left[1.12 + 0.61\cos(\beta_{in})\frac{\Delta V_{\theta}}{V_{in,ref}\sigma}\right] \qquad (A1)$$

where β_{in} is relative tangential inlet flow angle and $V_{in,ref}$ is the relative velocity into the blade row.

Appendix B: Setting Solidity using H_{te}

Alternatively the blade row solidity can be set by holding constant the suction-surface boundary layer shape factor at the trailing edge H_{te}. A program was written by To [16], to find the optimum aerofoil profile that yields the lowest profile loss.

Appendix C: Low Order Profile Loss Model

To calculate the lost efficiencies in section 3.3 only, a low order loss model is used. Equation 8 in [4] correlates the equivalent diffusion ratio $D_{eq}{}^{*}$ against the wake momentum thickness $(\theta/c)_2$. Using this value of $(\theta/c)_2$ and knowledge of the stage velocity triangles and solidities, equation 11 in [4] can be used to estimate the blade row total-pressure loss coefficients $\tilde{\omega}$. The stage lost efficiency can then be calculated from:

$$\frac{T\Delta s}{\Delta h_0} = \frac{2\left(W_{in,rotor}^2\tilde{\omega}_{rotor} + V_{in,stator}^2\tilde{\omega}_{stator}\right)}{\Delta h_0} \qquad (C1)$$

Appendix D: Low Order Endwall Loss Model

The total entropy generation, per unit pitch, in either the hub or casing endwall, can be calculated by:

$$\dot{S} = L\int_0^1 \frac{C_d\rho V_0^3}{T}\,d\left(\frac{x}{L}\right) \qquad (D1)$$

where L is the stage length and V_0 is the boundary layer edge velocity. Writing equation D1 in the form of lost efficiency gives:

$$\left(\frac{T\Delta s}{\Delta h_0}\right)_{endwall} = 2\frac{C_0}{V_x}\frac{L}{\Delta r}\int_0^1 C_d\left(\frac{V_{0,ref}}{C_0}\right)^3\frac{dx}{L} \qquad (D2)$$

where L is the stage length and $V_{0,ref}$ is the boundary layer edge velocity relative to the endwall.